Bragg Lasers up to the 400th Bragg Order with an Organic Active Layer

Yun Li,[1] Girish Lakhwani[1] *

[1] ARC Centre of Excellence in Exciton Science, School of Chemistry, University of Sydney. NSW 2006, Australia

[2] The University of Sydney Nano Institute, Sydney, NSW 2006, Australia

[3] Institute of Photonics and Optical Science, The University of Sydney. NSW 2006, Australia

*Author to whom correspondence should be addressed: girish.lakhwani@sydney.edu.au

Abstract

The output characteristics and lasing threshold behaviour of higher order Bragg lasers is explored using an organic active layer spin-cast over substrate-defined fused-silica gratings. Gratings ranging from 1st to the 400th Bragg order of varying duty cycle are fabricated with standard e-beam lithography. Distinct diffraction orders are observed at lower Bragg orders but smears out towards higher orders due to overlapping diffracted orders. Significant variation in thresholds is observed with duty cycle for most Bragg orders. A dramatic reduction in threshold is observed with increasing cavity length. The lowest lasing thresholds obtained for 4th and 400th order distributed feedback (DFB) lasers are ~1.4 μJ cm^{-2} and 4 μJ cm^{-2}, respectively, using $F8_{0.9}BT_{0.1}$ as an active layer. 400th order Bragg lasers are fabricated with direct-write photolithography using a UV laser diode, with comparable thresholds to e-beam lithography fabricated devices.

Introduction

Concerted efforts to increase the viability of simple fabrication, low-cost solid-state lasers has rapidly advanced the performance of non-conventional semiconductor materials such as organics, with respect to degradation and laser thresholds[1-3]. Distributed feedback

(DFB) and distributed Bragg reflector (DBR) resonators are typically used for organic lasers[2, 4, 5], and provide feedback at the Bragg condition

$$m\lambda = 2n_{eff}\Lambda, \quad (1)$$

where m is the Bragg order, λ is the targeted lasing wavelength, n_{eff}, is the modal effective refractive index of the resonator mode, and Λ is the periodicity of the grating. Lower order (m = 1, 2) lasers are used for their lower reported lasing thresholds[2, 4-6], however, high-resolution patterning by electron-beam lithography or interference lithography is required[7-9]. These patterning methods are limited by low throughput and poor control over resonator profiles respectively. At sufficiently high m, the fabrication capability can expand to UV photolithography (UV-PL), which combines high-throughput, potential fine-control of resonator features and low cost. The common perception is that with higher m, the laser threshold generally increases. However, the relative increase in threshold between successive m in literature is widely inconsistent for organic lasers[7, 8, 10-12].

For epitaxial group (III -V) semiconductors, significantly disparate m (m = 7, 25) Bragg lasers have been shown to produce near identical lasing thresholds under specific grating duty cycles (γ) and m. Numeric calculations showed that high mirror reflectivity could only be achieved in a small tuning range around 90 % fill factor for the high refractive index portion of the gratings, elsewhere, the reflectivity vanishes.[13-16] This observed dependence on γ has been attributed to the interaction of out-of-plane diffracted radiation from the coupled counter-propagating modes and partial waves, against the same coupled modes in the periodic waveguide[14, 17].

Here, the output characteristics and lasing threshold behaviour of higher order Bragg lasers is explored using a spin-cast organic active layer of $F8_{0.9}BT_{0.1}$ over substrate-patterned fused silica gratings. Gratings ranging from 1st to the 400th Bragg order of varying γ are

fabricated with standard e-beam lithography (EBL). Distinct diffraction orders can be identified for m < 100 lasers, while the output is smeared out for m >100. Significant variation in threshold is observed with minor variations in γ for most m. A substantial reduction in lasing threshold for a 400th order DFB laser is achieved by increasing the cavity/excitation stripe length. It is shown that 400th order Bragg lasers can be fabricated with direct-write UV-PL using a UV laser diode, with comparable thresholds to EBL fabricated devices.

Results and Discussion

The schematic for an m^{th} order DFB laser is illustrated in Figure 1(a), with a sample 50th order grating fabricated with direct-write UV PL shown in Fig. 1(b). All laser devices were pumped from the backside and emission was collected normal to the substrate plane, as depicted in the experimental setup (Fig. S3). The lasers were fabricated using ~180 nm active layers of $F8_{0.9}BT_{0.1}$ with 60 nm deep SiO_2 gratings. The grating periodicity was set to multiples of 183 nm ($m = 1$) with a targeted lasing wavelength of ~560 nm at $n_{eff} = 1.50$. The excitation stripe widths were adjusted to match the grating line length (50 μm), while the stripe lengths were chosen to match the cavity length of the lasers unless otherwise stated.

At the Bragg resonance condition, the surface emission profile as shown in Fig. 1(a) is characterized by (refer to supporting information pg. 6 for more details)

$$m\left(\frac{n_c sin\theta_l}{n_{eff}} - 1\right) = 2l, \qquad (2)$$

where l is an integer representing the diffraction order, θ_l is the angle of the diffracted order and n_c is the refractive index of the medium above the grating (in this case it is the active layer, $n_c = 1.7$). Inspection of Eqn. 2, indicates that higher m permits more diffracted orders

l and vertical out-coupling ($\theta_l = 0$) can be achieved for $l = -\frac{m}{2}$, that is, for even m. In this study, only even m lasers were fabricated, ensuring a vertical output is always present.

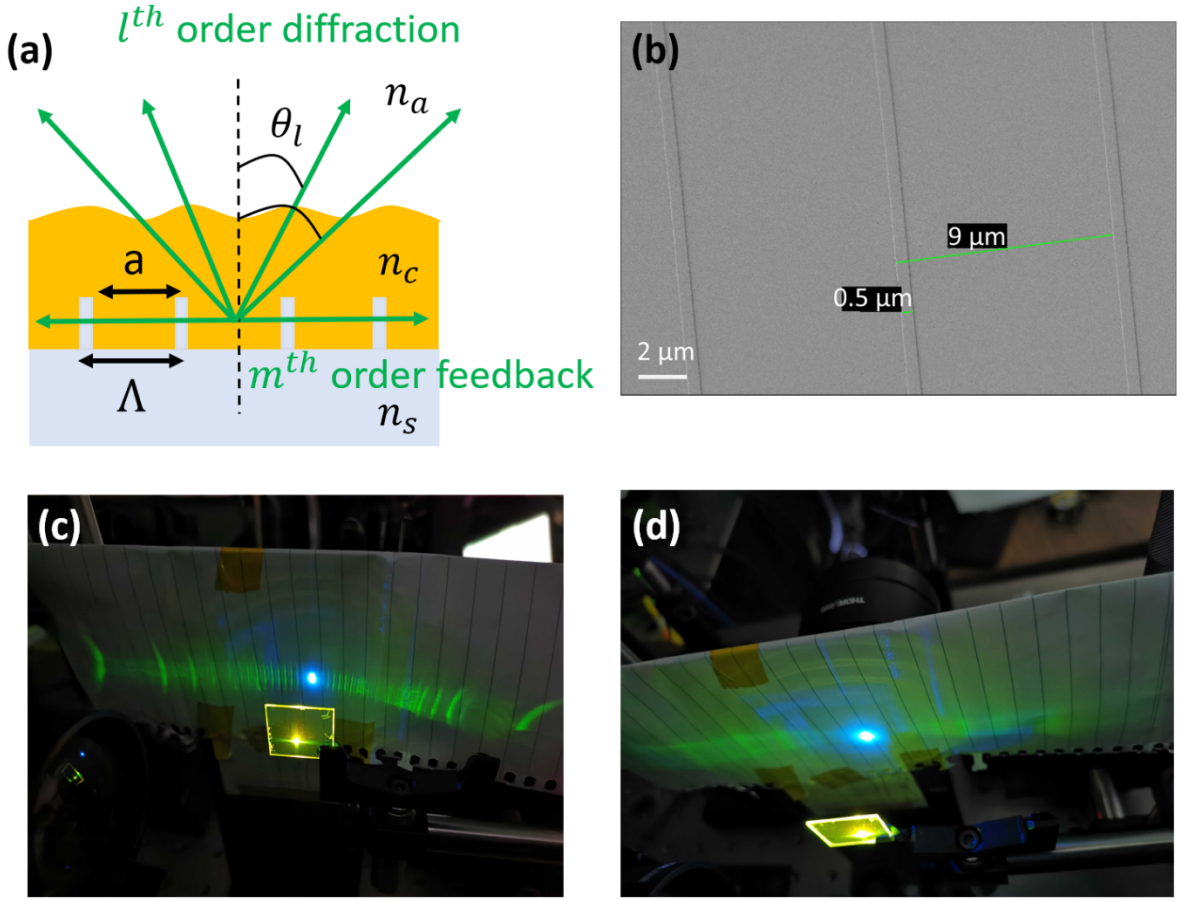

Fig. 1. (a) Schematic of higher order DFB laser (b) SEM image of 50th order 60 nm deep SiO_2 gratings fabricated with direct-write photolithography. (c) Pictogram of emission output from (c) 50th order and (d) 400th order DFB lasers far above lasing threshold observed at a distance ~ 4.5 cm from the sample.

Multiple distinct diffraction bands were observed for the 50th order DFB lasers above lasing threshold shown in Fig. 1(c) as expected. For the 400th order, the diffraction bands were smeared out relative to the 50th order (Fig. 1(d)). This is consistent with a redistribution of outcoupled intensity at higher m into the multiple diffracted orders. The numerous

diffracted orders then overlap at these higher grating orders, resulting in the observed surface emission.

Fluence-dependent spectra for a 93 % γ 400th order DFB laser with 1600 µm excitation stripe (1830 µm cavity length) is shown in Fig. 2(a). The super-linear growth of a feature centered at 559 nm with full-width half-maximum (FWHM) ~0.7 nm was observed, which is approximately the resolution of the spectrograph. A tentative assignment of this feature is made to lasing due to DFB. Inspection of the background emission shows a broad (~ 70 nm FWHM) feature that grows roughly linearly with pump fluence, at all wavelengths, away from the narrow feature, we assign this to spontaneous emission from the active film.

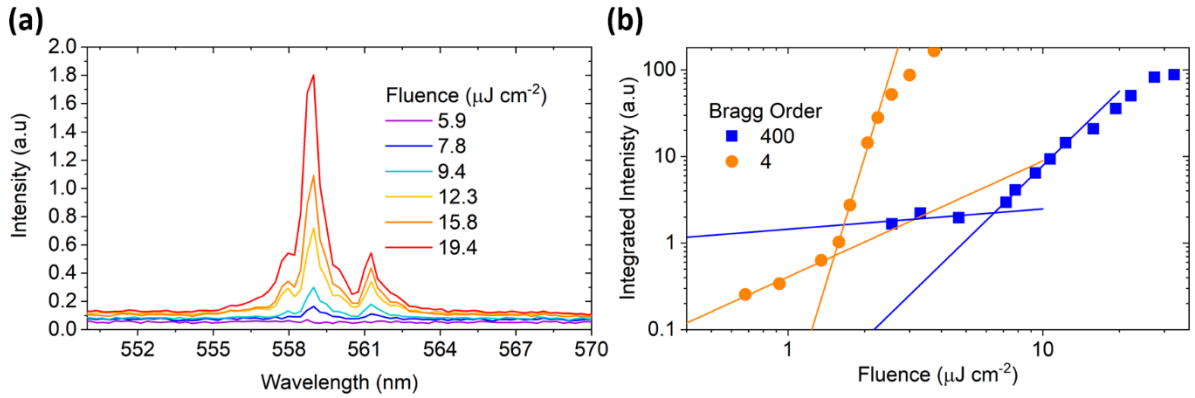

Fig. 2. (a) Typical spectral output of a 1.6 mm excitation stripe length 400th order, 93 % γ DFB laser for varying fluence. (b) Integrated (within 1.5 nm of main lasing peak) spectral intensity against fluence for 93 % γ, 0.4 mm long 4th, 1.6 mm long 400th order DFB lasers.

Amplified spontaneous emission (ASE) was not observed at appreciable intensities for fluences up to 33 µJ cm^{-2}. For reference, soft ASE thresholds for a 1 mm stripe is ~ 20 µJ cm^{-2} in the absence of the resonator. While the pump overlaps the DFB, the ASE intensity is potentially suppressed by radiation/scattering losses from the grating and lasing from the main resonator mode. Less prominent spectral features, immediately adjacent to the main lasing peak were observed, the relative intensities of these features did not grow in the same

way as the main peak and only appears with the onset of the main lasing peak. The relative intensities of the two peaks varied strongly with the lateral position of the spectrograph. Since several diffraction orders of varying angles are incident on the spectrograph, it is possible that these features stem from artefacts due to a stray diffraction order.

Typical integrated spectral intensities (within ± 1.5 nm of the main lasing peak) against fluence are given in Fig. 2(b) for 400th order (1.6 mm, 93 % γ) and 4th order (0.4 mm length, 93 % γ) lasers. At higher fluence, the intensity of the main lasing mode saturates. We attribute this primarily, to the oscillation of the second longitudinal mode on the opposing photonic band edge. This is indicated by the emergence of secondary peak/shoulders, adjacent to, and overlapping the main lasing mode (Fig. S5) for both 4th and 400th order lasers. The main stopband for 4th order lasers could be identified (Fig. S6), where lasing initially emerges on the long-wavelength band-edge, however, owing to the lower coupling coefficients at higher Bragg orders, the stopband could not be identified for the 400th order laser. Initial thresholds of ~6.4 μJ cm^{-2} and ~1.4 μJ cm^{-2} were identified for 400th and 4th order lasers respectively, however, values are subject to sample averaging.

For a pure square-periodic grating profile, the coupling coefficient is estimated by[18]

$$\kappa \propto \left| \frac{k_0 (n_2^2 - n_1^2) \Gamma_g}{2 n_{eff} \pi m} \sin\left(\frac{\pi m a}{\Lambda}\right) \right|, \quad (3)$$

where k_0 is the wavevector in vacuum, Γ_g is the confinement factor in the grating region, n_2/n_1 are the refractive indices of the materials comprising the grating and a is the grating linewidth of the higher refractive index material. Eqn. 3 implies a strong dependence on $\gamma = \frac{a}{\Lambda}$ and m, with all other parameters unchanged. In addition, with increasing m, the increase in number of radiating orders and partial waves are expected to modulate κ-dependence on γ to a greater extent as previously noted[14, 17]. Practically, the exact γ will not be produced

precisely, particularly at the 4th order and lower, due to the fabrication limitations, nevertheless, the results should capture the relative effect of changing γ.

The effect of γ and m on DFB and DBR laser thresholds is shown in Fig. 3(a) and (b) respectively. The excitation stripe lengths were fixed to approximately 400 and 1000 µm respectively for DFB and DBR lasers. For DFB lasers, this does not match the physical extent of the lasers, as the Bragg periods do not add up to exactly 400 µm, and was chosen as an initial test length to save fabrication time. DBR cavity lengths were limited to 1000 µm, as lasing thresholds cease to decrease beyond this length and to minimize losses due to ASE. The number of mirror periods were fixed to 25 in DBR lasers for $m \geq 4$ as lasing thresholds do not decrease further with increasing periods as shown in Fig. S8(a). For 1st order lasers, a 70 % γ, 40 period 2nd order out-coupler is included in the total cavity length which is placed between 1st order gratings for DFBs and at one of the mirror facets in DBRs.

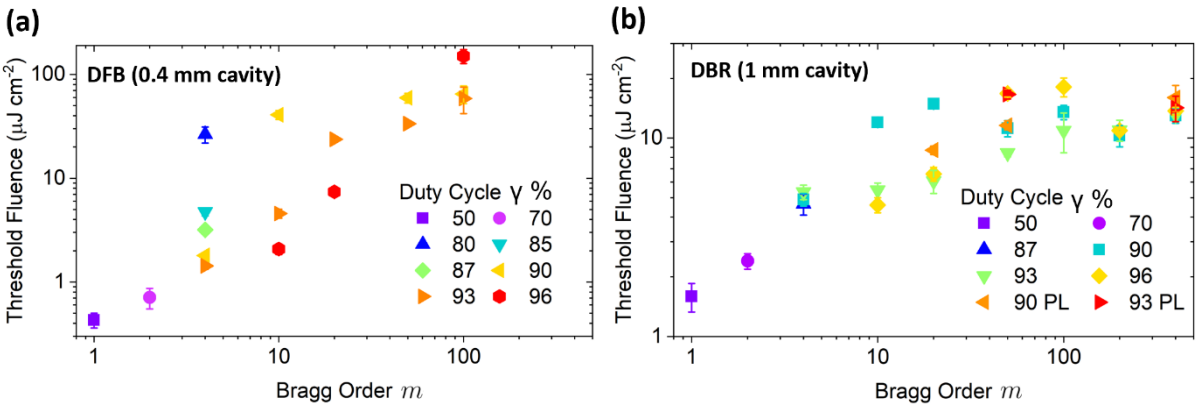

Fig. 3. Threshold fluences against Bragg order for varying grating γ for (a) ~400 µm cavity length DFB laser and (b) ~1000 µm cavity length DBR laser. Data points are omitted where threshold is not reached.

For DFB lasers, a dramatic reduction in lasing threshold was observed from 80 % γ (26.4 ± 4.6 µJ cm^{-2}) to 93 % γ (1.43 ± 0.10 µJ cm^{-2}) for 4th order lasers, with a continuous decrease in threshold for γ in-between. Beyond 93 % γ, we were unable to fabricate 4th order laser reliably due to the small linewidths required. At and below 75 % γ, lasing thresholds

were not reached before the film was ablated. Inspection of the $\sin\left(\frac{\pi m a}{\Lambda}\right)$ term in Eqn. 3 (plotted in Fig. S9), suggests that maximum κ, should have occurred at 87 % γ, however, the further decrease in threshold observed beyond 87 % γ suggests otherwise. The observed behavior is, however, consistent with the resonator mode being modulated by back-scattered radiation. However, the degree to which the modulation occurs, is predicated on numeric calculations and modelling.

For 10th and 20th order lasers, similar trends were observed, with decreasing threshold towards higher γ (thresholds are not reached in 90 % γ 20th order lasers). The exceptionally high thresholds at 90% γ can also be partially attributed to a null in κ for the two orders (Fig. S9). For the same reason, the lasing threshold is significantly higher at 96 % γ for the 50th and 100th orders. For 400 μm cavity lengths, lasing was not observed for $m > 100$ lasers, while in general, we observe an increase in lasing threshold for increasing Bragg order. This is expected based on a reduction in κ, corresponding to an increase in resonator end losses. The increase in threshold can also be attributed to increased propagation loss (~10 cm^{-1}) at higher m. Propagation loss increases, since the resonator mode must propagate further before being Bragg scattered at each period as shown in Fig. S10. Although DFB lasers could be fabricated down to the 20th order with UV-PL, the thresholds varied strongly with repeat fabrication owing to the high sensitivity in γ.

DBR thresholds increase with increasing m for all γ (Fig. 3(b)), as with DFB lasers. However, DBR lasing thresholds were less sensitive to both m and γ than their DFB counterparts. Since the periods were selected well above the saturation point of maximum reflectivity with respect to number of periods (Fig. S8(a)), reflectivity is not significantly influenced by un-optimized κ. Consequently, DBR lasers could be fabricated up to the 400th order with thresholds ~14 μJ cm^{-2}, and thresholds from UV-PL lasers were relatively reproducible upon repeat fabrication down to 20th order, with comparable thresholds to EBL-

fabricated lasers. Instead, we anticipate that higher thresholds will stem primarily from increased propagation loss at lower κ due to increased mirror penetration depth as shown in Fig S10.

The effect of cavity length on thresholds for a 400th order DFB laser is examined. Instead of using a pure DFB laser, an excitation stripe of variable length was positioned along a fixed 25 period grating. In this configuration, the laser operates as a hybrid distributed Bragg reflector (DBR)-DFB laser, where the unpumped grating section reflects light back into the pumped DFB section, where DFB occurs. This configuration is common in reports of DFB lasers where the grating area is larger than pump spot size. For a 400 μm stripe, two excitation geometries are tested, as depicted in Fig. 4(a). One, where the excitation stripe is positioned at the edge of the grating, and the other, when positioned in the middle of the grating. For the former case, reflection outside the DFB section only occurs from a single side, whereas in the latter, reflection occurs on both sides. For all other stripe lengths, the stripe is positioned in the middle section as illustrated in Fig. 4(b).

Recall that threshold was not reached for a pure 400 μm stripe that lack supporting mirrors. When positioned in the edge configuration, lasing was recovered as shown in Fig. 4(c). When positioned in the middle of the grating, a further 3-fold reduction in threshold was observed for 400 μm stripes at all γ. The difference in threshold is attributed to lesser resonator end losses as described above.

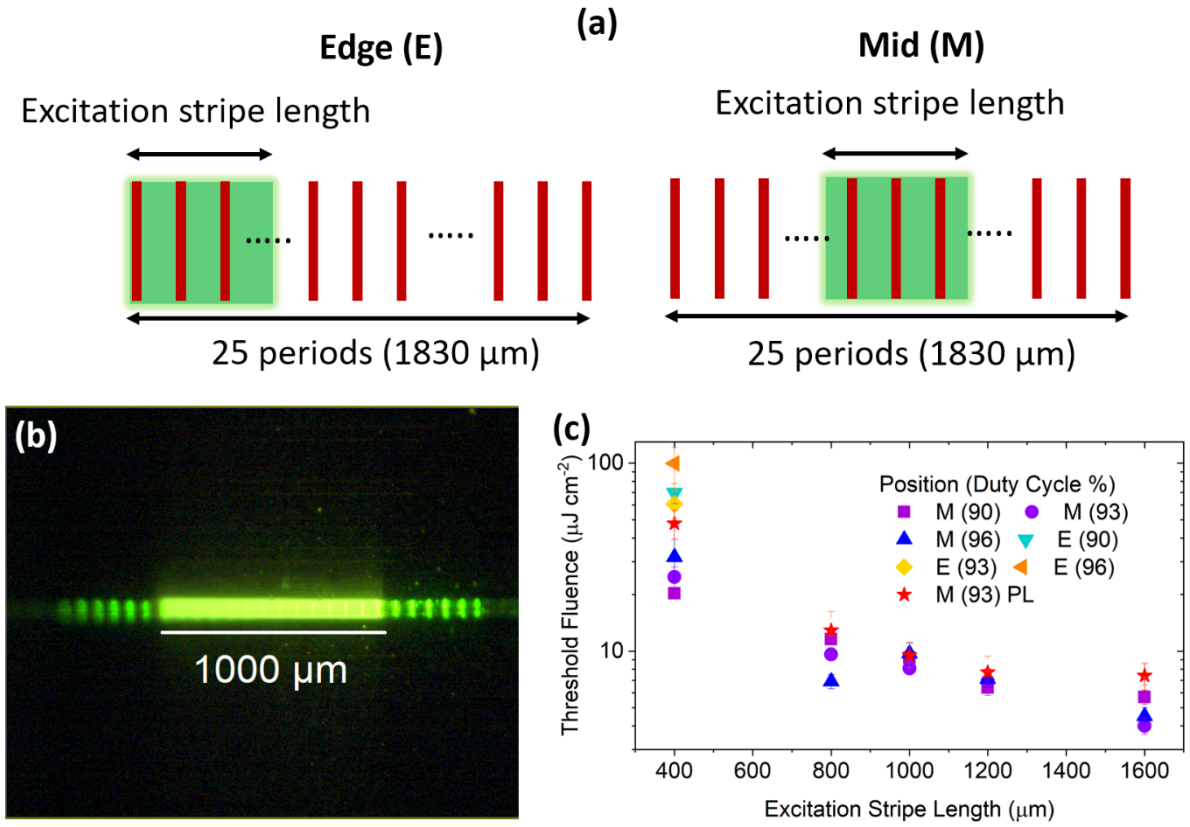

Fig. 4. (a) Schematic of edge (E) and mid (M) excitation stripe position used to measure lasing thresholds for a 400th order, 25 period (1830 µm) DFB laser. (b) Zoom lens image at oblique incidence of a 1000 µm (M) excitation stripe length on a 400th order DFB laser. (c) Threshold Fluence against excitation stripe length for E and M configurations of a 400th order DFB laser, with UV-PL defined gratings for comparison.

As the excitation stripe length was increased, contributions due to reflections from unexcited grating section was reduced and redirected into DFB. A decrease in threshold fluence was observed upon increasing the excitation stripe length and similar thresholds are found with UV-PL defined DFB lasers. For a 93 % γ grating, the threshold reduces from 24.8 ± 3.2 to 4.0 ± 0.4 µJ cm^{-2} between 400 µm and 1600 µm stripe lengths, surpassing the lowest thresholds found in 400th order DBR lasers. To explain this result, we look at an equation derived from coupled-wave theory for DFB lasers[19]. In the high gain

approximation ($\alpha \gg \kappa$), which should be true for higher m, we expect the threshold lasing condition to follow the implicit equation[19, 20],

$$|\kappa| \approx 2\alpha e^{-\alpha L}. \quad (4)$$

Here, α is the average electric-field gain coefficient of the active layer at threshold and L the cavity length. Since κ is a fixed property of the grating, an increase in L must be followed by a decrease in α (Fig. S11), which is consistent with the results obtained here. Physically, the reduction in threshold occurs due to increased total reflectivity and reduced resonator end losses.

We anticipate further reductions in thresholds are possible with higher stripe and cavity lengths but will saturate at some point due to over-coupling at high κL or from ASE[20, 21]. This saturation behavior was observed at shorter cavity lengths (~ 400 μm) for 4th order lasers, owing to their higher κ (Fig. S12(b)). Besides saturation effects, propagation loss for long grating periods, ultimately sets a lower limit on the lasing thresholds, in addition to radiation loss. Moreover, the length over which the excitation stripe is roughly homogenous, is limited by the finite size (~1 cm) of the gaussian pump beam, which forms the stripe via a slit and a cylindrical lens as described in Fig. S3.

From inspection, Eqn. 4 implies that relatively large changes to κ, results in significantly lesser changes to α due to the exponential factor. This accounts for why, at higher Bragg orders (for optimized cavity lengths), a substantial increase to lasing thresholds is not observed. It is, however, somewhat surprising that despite the expected sinusoidal dependance of κ on γ (Eqn. 3), which oscillates with higher frequency with respect to γ, that the thresholds are relatively low and as insensitive as they are to varying γ at higher Bragg orders. Given the relative invariance to γ with the 400th order, it would be interesting to see how low γ can be pushed before observing a significant increase to threshold. In this respect,

numeric calculations on models that involve modifications to the resonator mode via radiation/partial waves at these high m, would help to elucidate the origin of the observed behaviour.

To conclude, DFB lasers were fabricated using e-beam lithography up to the 400th order. At lower m, distinct diffraction orders were observed. However, at higher m, the output emission was smeared out due to redistribution of intensity into multiple overlapping diffraction orders. This could be useful in applications requiring wide angle, spatially homogeneous, monochromatic sources. The thresholds were found to be strongly dependent on both m and γ, where lasing thresholds generally increase with m and have a complex dependence on γ. A substantial reduction in lasing threshold was observed upon increasing the cavity length for a 400th order DFB laser. The lowest thresholds obtained for 4 and 400th order lasers were ~1.4 and 4 μJ cm^{-2} respectively. Lasing was observed in 400th order DFB lasers using direct-write UV-PL with a laser diode, with comparable thresholds to EBL fabricated lasers. To elucidate the throughput potential, for the same patterns, a total write time of ~3 min was required with the UV-PL system, while EBL requires ~ 3 hrs.

[1] C. Adachi,A. S. Sandanayaka, *CCS Chemistry* **2020**, *2(4),* 1203.

[2] A. J. Kuehne,M. C. Gather, *Chemical Reviews* **2016**, *116(21),* 12823.

[3] I. D. W. Samuel,G. A. Turnbull, *Chemical Reviews* **2007**, *107(4),* 1272.

[4] Q. Zhang, W. Tao, J. Huang, R. Xia,J. Cabanillas-Gonzalez, *Advanced Photonics Research* **2021**, *2(5),* 2000155.

[5] S. Chénais,S. Forget, *Polymer International* **2012**, *61(3),* 390.

[6] C. Karnutsch, C. Pflumm, G. Heliotis, J. C. deMello, D. D. C. Bradley, J. Wang, T. Weimann, V. Haug, C. Gärtner,U. Lemmer, *Applied Physics Letters* **2007**, *90(13),* 131104.

[7] M. Liu, Y. Liu, G. Zhang, Z. Peng, D. Li, J. Ma,L. Xuan, *Journal of Physics D: Applied Physics* **2016**, *49(46),* 465102.

[8] P. Zhou, L. Niu, A. Hayat, F. Cao, T. Zhai,X. Zhang, *Polymers* **2019**, *11(2),* 258.

[9] H. Kogelnik,C. Shank, *Applied Physics Letters* **1971**, *18(4),* 152.

[10] Z. Li, Z. Zhang, T. Emery, A. Scherer,D. Psaltis, *Optics Express* **2006**, *14(2),* 696.

[11] S. Balslev,A. Kristensen, *Optics Express* **2005**, *13(1),* 344.

[12] N. Tsutsumi, K. Kaida, K. Kinashi,W. Sakai, *Scientific Reports* **2019**, *9(1),* 10582.

[13] J. Fricke, H. Wenzel, M. Matalla, A. Klehr,G. Erbert, *Semiconductor Science and Technology* **2005**, *20(11),* 1149.

[14] V. V. Zolotarev, A. Y. Leshko, N. A. Pikhtin, S. O. Slipchenko, Z. N. Sokolova, Y. V. Lubyanskiy, N. V. Voronkova,I. S. Tarasov, *Quantum Electronics* **2015**, *45(12),* 1091.

[15] J. Fricke, W. John, A. Klehr, P. Ressel, L. Weixelbaum, H. Wenzel,G. Erbert, *Semiconductor Science and Technology* **2012**, *27(5),* 055009.

[16] J. Fricke, A. Klehr, O. Brox, W. John, A. Ginolas, P. Ressel, L. Weixelbaum,G. Erbert, *Semiconductor Science and Technology* **2013**, *28(3),* 035009.

[17] W. Streifer, D. Scifres,R. Burnham, *IEEE Journal of Quantum Electronics* **1977**, *13(4),* 134.

[18] W. Streifer, D. Scifres,R. Burnham, *IEEE Journal of Quantum Electronics* **1975**, *11(11),* 867.

[19] J. E. Bjorkholm,C. V. Shank, *Applied Physics Letters* **1972**, *20(8),* 306.

[20] H. Kogelnik,C. Shank, *Journal of applied physics* **1972**, *43(5),* 2327.

[21] E. M. Calzado, J. M. Villalvilla, P. G. Boj, J. A. Quintana, V. Navarro-Fuster, A. Retolaza, S. Merino,M. A. Díaz-García, *Applied Physics Letters* **2012**, *101(22),* 223303.